Atomic Force Microscopy under Controlled Conditions Reveals Structure of C-Terminal Region of α-Synuclein in Amyloid Fibrils

Kim K. M. Sweers,[†] Kees O. van der Werf,[†] Martin L. Bennink,[†,*] and Vinod Subramaniam[†,‡,*]

[†]Nanobiophysics, MESA+ Institute for Nanotechnology and [‡]MIRA Institute for Biomedical Technology and Technical Medicine, Faculty of Science and Technology, University of Twente, Enschede, The Netherlands

ABSTRACT

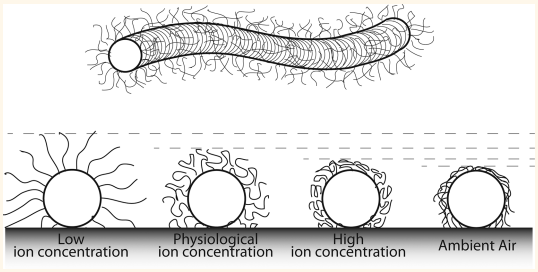

Atomic force microscopy (AFM) is widely used to measure morphological and mechanical properties of biological materials at the nanoscale. AFM is able to visualize and measure these properties in different environmental conditions. However, these conditions can influence the results considerably, rendering their interpretation a matter of some subtlety. We demonstrate this by imaging ~10 nm diameter α-synuclein amyloid fibrils, focusing specifically on the structure of the C-terminal part of the protein monomers incorporated into fibrils. Despite these influences leading to variations in fibril heights, we have shown that by maintaining careful control of AFM settings we can quantitatively compare the morphological parameters of fibrils imaged in air or in buffer conditions. From this comparison we were able to deduce the semiflexible character of this C-terminal region. Fibril height differences measured in air and liquid indicate that the C-terminal region collapses onto the fibril core upon drying. The fibril heights decrease upon increasing ion concentration in solution, suggesting that the C-terminal tails collapse into more compact structures as a result of charge screening. Finally, PeakForce QNM measurements show an apparent heterogeneity of C-terminal packing along the fibril length.

KEYWORDS: atomic force microscopy · amyloid fibrils · α-synuclein · PeakForce QNM · peptide truncation

Atomic force microscopy (AFM) is a powerful tool to investigate morphological and mechanical properties of nanoscale biological materials in their near-native environment. AFM-based approaches have yielded structural and functional insights into the aggregation of proteins into amyloid fibrils, reviewed, for example, in Gosal *et al.* and Knowles *et al.*[1,2] Amyloid fibrils of several proteins are related to the development of neurodegenerative diseases. One example of such a disease-related protein is the human α-synuclein (αSYN) protein, which forms amyloid fibrils that are implicated in Parkinson's disease.[4,5] Several AFM-based morphological studies on αSYN fibrils have been reported in the literature, comparing fibrils formed from different mutants of αSYN. Different structural models have been derived from these data.[5−7] The height of fibrils formed from wild-type αSYN found in several previously reported studies ranges from 5 to 15 nm, which can be attributed to the significant morphological diversity of the fibrils formed (polymorphism), but also to variations in the AFM scanning conditions; see Figure 1.

One aspect influencing the morphology of protein aggregates and other biological samples measured with AFM that is often neglected is the role of the underlying substrate and the surrounding medium. Substrate influences have been studied previously where, for instance, tuning the hydrophobicity of the surface alters the propensity for IAPP monomers to aggregate in amyloid fibrils.[22] In contrast to other nanometer-scale imaging techniques (such as electron microscopy), an innate advantage of AFM is its ability to image biological samples in physiologically relevant solutions. The AFM mode commonly used with biological samples is tapping or intermittent mode, which can be used in both ambient air and liquid conditions. However, tip−sample interactions are very different for both media, resulting in large morphological differences of nanometer scale features. As a result of this difference in interaction forces, different driving amplitudes and force set points have to be used to optimally image the

* Address correspondence to m.l.bennink@utwente.nl; v.subramaniam@utwente.nl.

Received for review February 27, 2012 and accepted June 13, 2012.

Published online June 13, 2012
10.1021/nn300863n

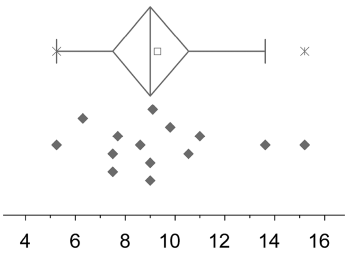

Figure 1. Box-and-whisker diagram indicating the spread of fibril height data found in the literature measured with AFM or transmission electron microscopy for wild-type α-synuclein.[5−21] Plot indicates sample minimum, maximum, and median (vertical lines), outliers (crosses), and the average of all data points (open square).

fibrils. This leads to differences in morphological parameters, such as the fibril height. Furthermore the cantilever behavior is very different for both media. The hydrodynamic damping and the extra apparent mass attributed to the displaced liquid cause the resonant frequency to reduce 3-fold and lower the Q-factor significantly.[23] In addition, when the cantilever is actively driven in a liquid cell, the liquid droplet and cell chamber could add more resonances, which requires some trial and error to find the correct resonant frequency for operation. These differences in operating frequencies can also induce differences in fibril morphology. For instance, the apparent amyloid fibril diameter has been reported to decrease in one study[24] and increase in another[25] when imaged in ambient air compared to liquid conditions. Also with piezoresponse force microscopy the apparent amyloid fibril height and width decrease significantly when imaged in air compared to liquid.[26]

In this study we have imaged αSYN amyloid fibrils using tapping mode AFM imaging in different environmental conditions. We showed that with careful control of the operating parameters the fibril morphology measured in different environmental conditions could shed light on the structure of the C-terminal region in αSYN amyloid fibrils.

Human αSYN is a small 140 amino acid protein associated with Parkinson's disease.[2,3,27] αSYN forms fibrils of around 10 nm in diameter and displays a periodic height variation along its length, attributed to a twisted structure. The C-terminal region is believed to be unstructured in both monomeric and fibrillar form and is highly negatively charged. The C-terminus consists of ∼40 amino acids, which, when fully extended, correspond to a length of ∼15 nm. In this study we have studied the effect of the surrounding medium on the structure of the C-terminal part of the protein when aggregated into amyloid fibrils. To this end we used full-length wild-type protein and the disease-related mutant E46K, bearing a point mutation located in the fibril core.[28] The E46K mutant is expected to have a similarly unstructured C-terminus to the wild-type protein. We furthermore investigated fibrils generated

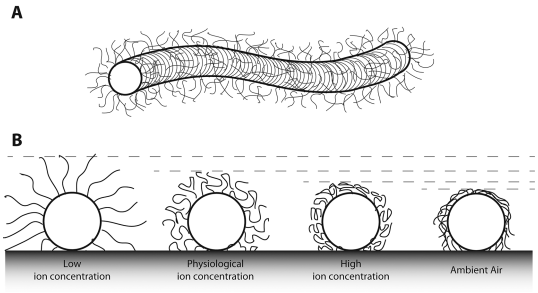

Figure 2. (A) Schematic representation of a fibril with stacked β-sheet folded monomers perpendicular to the fibril axis and an unstructured C-terminus outside the fibril. (B) Different conformations of C-terminal tails outside the fibril core in liquid conditions with different ion concentrations and in ambient air.

from a C-terminally truncated variant, αSYN(1−108), comprising amino acids 1−108.

We hypothesize that the C-terminus is unstructured and is exposed on the surface of the fibril, analogous to a polymer brush (Figure 2A). The structure of the C-terminus within this polymer brush can be influenced by different environmental conditions (Figure 2B). First, the C-terminal tail could collapse upon drying of the fibril. To measure this collapsing effect upon drying, we measured the difference in fibril heights of full-length and C-terminus-truncated α-synuclein fibrils under different solution conditions. The height reduction due to the C-terminal region collapsing onto the fibril core is, as expected, more apparent in full-length variants, the wild-type and E46K fibrils, than in the C-terminus-truncated variants. Second, the C-terminal brush on the fibril exterior is likely to differ in size as a function of the extent of charge shielding by ions in the solution. This could create fibril height differences at different ion concentrations measured with AFM. Finally, we test whether the polymer brush is uniformly structured along the fibril length. We expect that different tip−sample interactions can be at least partially visualized by making force distance curves on the fibrils. In this study we used PeakForce QNM to rapidly acquire force distance curves and map different surface properties such as adhesion and modulus of elasticity derived according to the Derjaguin−Muller−Toporov (DMT) model.[29,30] This newly introduced technique has already been used to characterize mechanical properties of polymers, nanosheets, and amyloid fibrils.[21,31−33] Here, we use the method to map differences in interaction forces between the substrate and fibril and along the fibril axis.

RESULTS AND DISCUSSION

Wild-Type and 1−108 α-Synuclein Aggregation. To obtain fibrils for wild-type and E46K αSYN, and truncated αSYN(1−108), the monomeric protein was left to aggregate for 72 h at 37 °C. The aggregation kinetics were monitored using Thioflavin T (ThioT), which is a

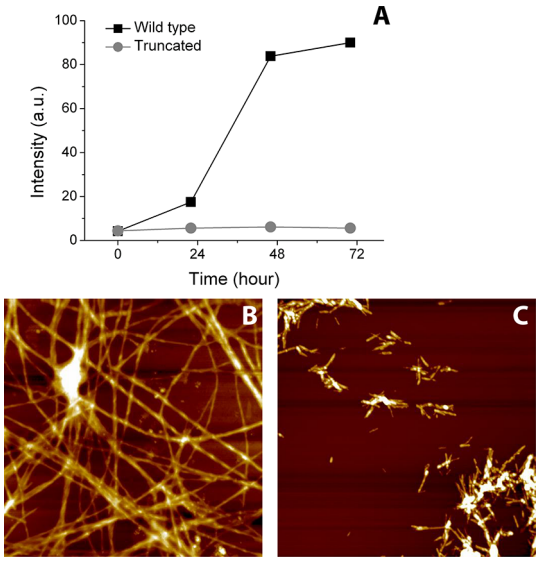

Figure 3. Aggregation of wild-type protein and C-terminally truncated αSYN(1−108). (A) Thioflavin T intensity curve shows hardly any intensity increase for αSYN(1−108). (B) Typical AFM image of wild-type fibrils after 48 h. (C) Typical AFM images of αSYN(1−108) fibrils after 48 h. Both AFM images are 5 × 5 μm, and *z*-range is 20 nm.

fluorescent dye that shows enhanced fluorescence upon binding to cross-β conformations characteristic of amyloid fibrils.[34] The aggregation reaction resulted in mature fibrils after 48 h for both full-length and truncated variants and was independently verified by AFM. In the ThioT intensity assay, a very small increase in ThioT fluorescence intensity was observed for the 1−108 variant compared to the full-length variants; see Figure 3. Previous studies have demonstrated that αSYN(1−108) aggregates significantly faster than wild-type αSYN.[16,35] Although a lack of ThioT fluorescence is commonly interpreted as the lack of amyloid structure, it has been observed previously that not all amyloid stains efficiently with ThioT.[36] It is possible that the removal of the negative charges present on the C-terminus influences the electrostatic interaction of the positively charged ThioT with α-synuclein. The AFM data very clearly show fibrillar structure for both wild-type and truncated protein; the latter have been demonstrated to have significant β-sheet content.[16] We thus believe the fibril cores for the wild-type protein and the 1−108 variant to be similar. The αSYN(1−108) fibrils are considerably shorter than the wild-type fibrils, but otherwise exhibited similar heights in liquid (Figure 3 and Table 1). E46K αSYN formed fibrils in the same time frame as the wild-type protein (kinetic data not shown).

AFM tapping mode images of fibrils formed with the full-length proteins and the truncated variant were recorded in buffer solution and ambient air conditions. Fibrils after 48 h incubation were deposited on the surface and imaged. The measured heights for all variants and imaging conditions are listed in Table 1.

TABLE 1. Fibril Height Data for Wild-Type, E46K, and αSYN(1−108) in Two Different Scanning Environments, Liquid and Ambient Air

	fibril height (nm), liquid	fibril height (nm), air	height reduction,[a] (%)
wild type	7.9 ± 0.4 (*N* = 150)	6.6 ± 0.9 (*N* = 151)	16
E46K	6.8 ± 1.3 (*N* = 72)	5.6 ± 1.1 (*N* = 62)	17
1−108 A	7.6 ± 1.9 (*N* = 105)	7.2 ± 1.8 (*N* = 64)	5
1−108 B	8.9 ± 2.3 (*N* = 106)	8.7 ± 2.5 (*N* = 72)	2

[a] Height reduction is given in percentage of the height measured in liquid.

Due to the very short lengths of fibrils formed by αSYN(1−108), it is difficult to obtain information on periodic height variations. In contrast, the wild-type fibrils do show a height variation along their length with a periodicity of around 50 nm, while the twist found for the E46K variant was a little smaller, around 45 nm, which are similar to values reported previously.[5,7]

Fibril heights obtained for the wild-type and E46K αSYN are similar to heights reported previously; see Table 1.[5,7,20] Determining whether the C-terminus of αSYN behaves as a polymer brush and thus increases the fibril height is not straightforward. The αSYN-(1−108) duplicates differ by 1.3 nm in height, which led to the wild-type αSYN heights being both higher and lower than those extracted from the individual measurement sets of the truncated variant. Murray *et al*. found no decreasing trend in αSYN fibril diameters with progressive C-terminal truncations. They found a diameter decrease of around 3.8 nm for 1−110 αSYN compared to the full-length protein. However, the 1−130 variant was similar in size to 1−110 αSYN, while 1−120 αSYN showed an increase in diameter compared to both other truncated variants.[16] Zhang *et al*. found a 30% height decrease for both a C- and an N-terminally truncated αSYN; however, the full-length fibrils already exhibited very low (6.5 nm) heights.[19] As seen in Figure 1, for wild-type αSYN, the spread of fibril heights reported in a range of AFM and TEM studies is considerable. This variation is most likely partly due to differences in the structure of the fibrils as a result of different aggregation conditions such as temperature, agitation methods, or buffers used. Another important factor is likely due to differences in AFM imaging conditions, such as the tapping amplitude, feedback settings, or environmental conditions. Even the choice of substrates onto which the fibrils are adhered could induce height differences.[37] Furthermore, the AFM tip radius can also influence height measurements, an effect that is particularly important for nanoscaled samples such as DNA.[38]

The differences in tip−sample interactions in ambient air and liquid conditions have been discussed in the literature.[39] One major difference is the thin water film on the substrate that is always present in dried samples (*i.e*., ambient air imaging) and whose

thickness depends on the ambient humidity.[40] When imaging in liquid, the adhesion forces that the tip experiences are only from the interaction of the tip and the surface, while when imaging in air, the tip experiences an additional adhesion resulting from the capillary force of the thin water film. Furthermore, in liquid the van der Waals forces are reduced 10-fold.[39,41] Both the absence of the water film and smaller van der Waals forces in liquid allow for lower tapping amplitudes and, thus, lower forces applied to the sample. The electrostatic forces depend on the charges of both the tip and the sample. In liquid this electrostatic interaction between the charges on the surface is modulated by counterions present in the solution, which form an electrostatic double layer. This force can be tuned by changing the ion concentration in the solution.[41]

The forces mentioned above influence fibril height measurements. We therefore systematically studied a number of different fibril samples (made from the full-length protein and the truncated version) using the same set of imaging parameters for all the measurements in air and another set of imaging parameters for all experiments in liquid. Different cantilevers were used for the air and liquid measurements. For all data sets, the tips used were relatively blunt (tip radius ~85 ± 10 nm) compared to the fibrils (diameter ~8 nm). Since the size of the fibrils is relatively large compared to DNA, and the blunt tips used have similar radii, we assume the influence of tip−sample geometry described by Santos *et al*. on the height differences to be similar for all data sets.[38] This selection of tips and of AFM settings allowed us to compare the relative height differences between the different fibril species. The fibril height obtained in air when compared to those obtained in a liquid environment is 17% lower, a difference that is similar to that reported previously for paired helical filaments.[24] The 17% height reduction is attributed to the collapse of the C-terminus onto the fibril core upon drying (see Figure 2B). In contrast to the full-length fibrils we measured a negligible height reduction (2−5%) for the 1−108 variant. We believe that the fibril core of αSYN(1−108) is expected to have a similar structure to those formed from the full-length protein. Furthermore this structure is densely packed, leaving little room for water within the fibril core.

AFM Measurements at Different Ion Concentrations: Tapping Mode and PeakForce QNM. The strongly negatively charged C-termini on the fibril exterior can be affected by the ionic strength of the buffer. When these negatively charged tails are charged and closely packed, they can be visualized as a polymer brush, where we expect the tails to extend radially from the fibril core (see Figure 2B), resulting in a larger fibril height. When the charges on the tails are screened, the C-termini are expected to collapse upon themselves, resulting in a more condensed structure and thus a lower fibril height (Figure 2B). To measure this effect, we have measured the fibril heights as a function of ion concentration in the surrounding buffer. After initial deposition of the protein fibrils on the substrate the surrounding solution was exchanged with a 10 mM Tris-HCl buffer. AFM images were made of at least 60 fibrils. Next the buffer was exchanged for one with a higher NaCl concentration and left to settle as described in the Materials and Methods section, and the same sample was imaged again. This procedure was repeated for every ion concentration.

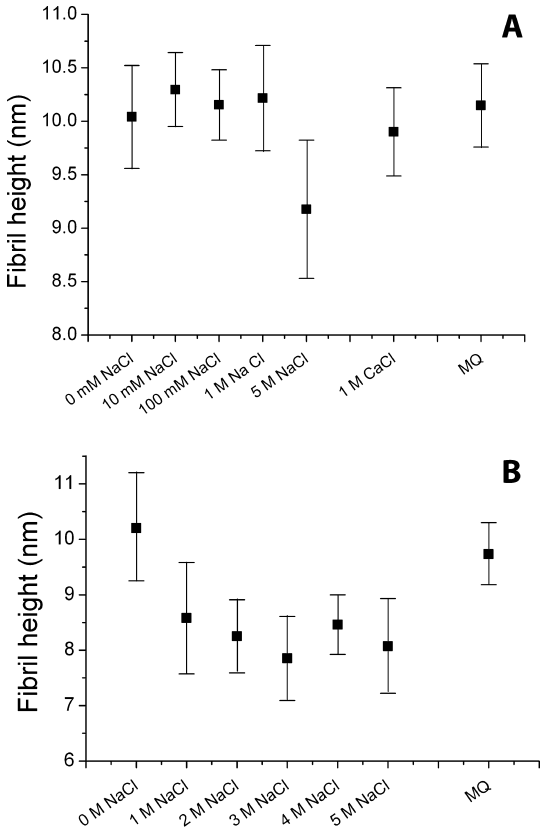

Figure 4. Wild-type fibril heights at different ion concentrations. (A) Experiments at lower ion concentrations, where no differences in fibril heights are seen. A clear height difference is observed at 5 M NaCl, and also a slight difference between 1 M NaCl and 1 M CaCl is seen. (B) Ion concentration series between 1 and 5 M NaCl. The height reduction is reversible, as shown by the last control experiment in Milli-Q, which restores the height to the initial value.

As a first experiment, we varied salt concentrations from 0 to 1 M NaCl, for which the heights of the protein fibrils did not significantly change (Figure 4A). We then introduced 5 M NaCl; in these conditions the height of the fibril showed a clear decrease of more than 1 nm. We also observed a small fibril height difference of ~0.3 nm depending on whether 1 M monovalent or 1 M multivalent salts were used. In the second experiment we systematically explored higher salt concentrations, from 1 to 5 M NaCl. As shown in Figure 4B, after 3 M NaCl there is no further height reduction found. To check whether these height differences are reversible,

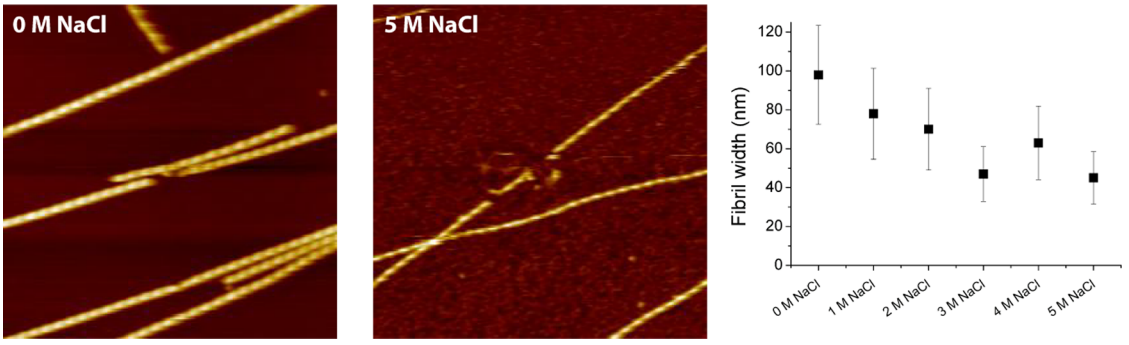

Figure 5. Typical images of wild-type fibrils measured at 0 and 5 M NaCl buffers and graph of fibril widths measured at different salt concentrations. The fibrils at 0 M NaCl appeared thicker compared to the fibrils measured at 5 M NaCl. Image size is 2 × 2 μm, 256 pixels, and *z*-range of 20 nm.

both experiments were terminated with measurements in ultrapure water, which restored the fibril height to the initial heights found at 0 M NaCl. Both experiments show a small variability between the same buffer conditions. The small differences are mainly caused by the use of different AFM cantilevers, which can influence the results slightly due to different contact areas, leading to small differences in tip−sample interactions.[38] The difference observed at 1 M NaCl between both experiments is considerable. We propose that the 1 M NaCl concentration could be around the transition point where the ion concentration affects the fibril height. It is possible that the local ion concentrations around the fibril for both experiments were not the same, causing the height difference between these experiments at 1 M NaCl. At higher salt concentrations, above 3 M NaCl, we do not observe any further differences in height. At these concentrations it is very well possible that the C-terminal tail is fully collapsed on the fibril due to salting-out of the protein.

We also observed an apparent increased lateral resolution of the images with increasing salt concentration (Figure 5). The fibrils not only decreased in height but also appeared thinner in the images, with widths of on average 50 nm at above 2 M NaCl concentrations, compared to 100 nm at 0 M NaCl. The interaction between the tip and the fibril decreases the fibril height and therefore also the fibril width. However, the decrease in fibril width is more than expected (50 nm decrease between 0 M NaCl and 3 M NaCl) based purely on this effect. A reduction of about 20% in height is expected to result in a 10% decrease in the width of the fibrils (assuming a tip radius of 85 nm). The observed 40−50% decrease in width can be explained by a decreased repulsive interaction between the negative tip and mica surface. When imaging a protein fibril, the interaction of the tip with the sample is a complex combination of the interaction of the tip with the fibril and of the tip with the underlying mica. At higher ion concentrations, the electrostatic repulsion between the tip and the mica and the fibril surface is reduced, making

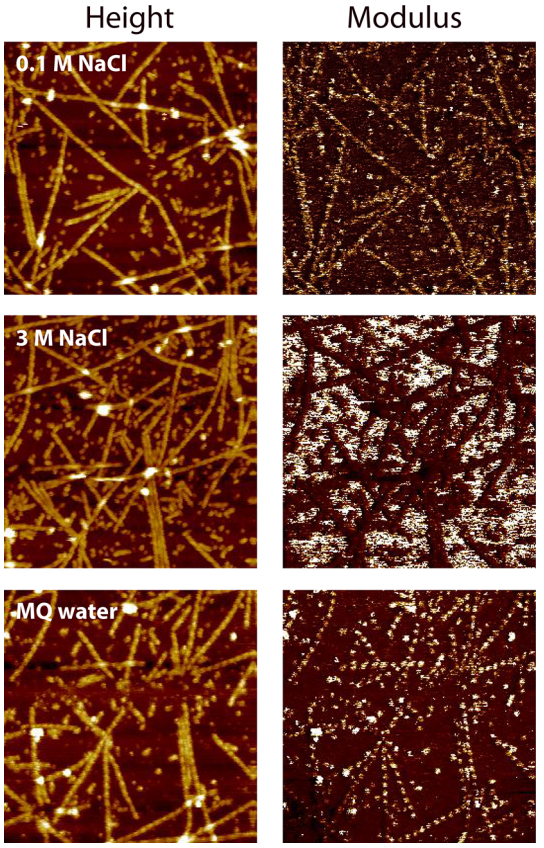

Figure 6. Height images and DMT modulus maps at the three different solution conditions. Images are 2 × 2 μm in size, and the *z*-range of the height images is 20−40 nm. For 0.1 M NaCl (upper panel) and Milli-Q water (bottom panel) the *z*-range of the modulus map is 60 MPa, while for 3 M NaCl (middle panel) the *z*-range is 500 MPa.

it possible for the AFM tip to follow the surface and fibrils more closely, thus enhancing the lateral resolution.

We also performed PeakForce QNM measurements of the same wild-type fibril sample under two different ion concentration conditions, namely, in Tris-HCl buffers containing 0.1 M NaCl or 3 M NaCl and finally in ultrapure water. PeakForce QNM uses force−distance curves at a rate of 1 kHz to determine several properties such as height, adhesion, and DMT modulus.[21,29] The height images with corresponding DMT modulus maps

are displayed in Figure 6. The topography images show that the fibril heights are similar to those found with tapping mode. Also, the periodic height variations are visible. The DMT modulus maps show large differences between the 0.1 M NaCl and the 3 M NaCl samples. The modulus value for the background mica changes from ~10 MPa at 0.1 M NaCl to ~500 MPa at 3 M NaCl. This results in an apparent contrast inversion when increasing and decreasing the ion concentration. The modulus values of the fibrils at all three buffer conditions are similar. However, at 0.1 M NaCl (and also at 0 M), the DMT modulus shows a periodic modulation along the fibril length, similar to that observed in the topography, which is not observed in the presence of 3 M NaCl. The extremely low modulus found for mica in 0.1 M NaCl is because the force set point used in PeakForce QNM was very low. In the case of mica, which is charged at low ionic conditions, this means that the part of the force curve that is used for determining the elastic modulus is dominated by the electrostatic repulsion and not the actual indentation of the material. For this reason the values of the DMT modulus obtained in these PeakForce experiments are not representative of the true elastic modulus of the material.

Increasing ion concentration in the scanning buffer decreased the fibril height by 1 to 2 nm and increased the lateral resolution. This is potentially due to two different effects. First, the ions shield the negative charges on the C-terminus, which decreases the repulsion between the different C-termini along the fibril length. This could cause the C-termini to collapse onto the fibril core. Whether the C-terminus actually behaves as a polymer brush depends on the radius of gyration of the C-terminus and the surface area of the fibril. An αSYN fibril consists of β-strand folded monomers that are stacked perpendicular along the fibril length with ~0.5 nm spacing of hydrogen bonds between the strands.[43,44] If we calculate the surface area of a small, 0.5 nm in height cylinder with a diameter of 10 nm, this surface area allows 2.6 to 3.9 nm^2 space per C-terminus, depending on whether we assume a packing model with 4 or 6 monomers per mature fibril. A 40 amino acid chain has a radius of gyration from 1.6 nm up to almost 6 nm depending on the solvent conditions.[45,46] These values indicate that we are at the boundary between a random coil and a polymer brush, where for different conditions either the random coil formation or an extended, polymer brush, conformation of the C-terminal tails would be favored. Second, the increased ion concentration decreases the electrostatic double-layer repulsion forces between tip and sample. This phenomenon can also be seen in the PeakForce QNM measurements. Here, due to the increased repulsion force between the tip and sample at lower ion concentrations, the negatively charged mica surface appears as soft as the fibrils. However, at the 3 M NaCl concentration, the mica appears stiffer compared to the fibrils. This effect has been shown before in various studies where the repulsion force clearly influences the slope of the force curve and is the same effect that causes the apparent increase in lateral resolution in the high ion concentration tapping mode experiments.[47−49] Interestingly, the PeakForce QNM measurements also show, at low ion concentrations, a periodic modulation of the measured DMT modulus along the length of the fibril (see Figure 6). This same modulation was also observed in the adhesion (data not shown). At this point it is not clear whether this periodic modulation in DMT modulus and adhesion is caused by the heterogeneity in the C-terminal brush or the contact area between tip and sample or a combination of both. However, with this imaging mode it may be possible to shed light on the brush distribution from charge interactions or on the helical shape of the fibril from the tip−fibril contact area causing different adhesion forces.

CONCLUSION

We observed that α-synuclein fibrils imaged in air appear around 17% lower in height compared to the same fibrils imaged in liquid environment. The truncated α-synuclein variant shows only up to 2−5% height decrease upon drying. This height difference of the α-synuclein fibrils is most probably the result of the collapse of the C-termini on the fibril core as the sample is dried.

Besides changes in the structure of the protein fibril as a result of a change in the environment, also the interactions between the tip and the sample change for different environmental conditions, which can lead to a different height when imaged with AFM. We show that the height decrease of α-synuclein fibrils imaged in different salt concentrations ranging from 0 to 5 M NaCl can be as much as 20%. This height decrease can be attributed to shielding of negative charges on the C-terminus. Aside from the height decrease, the fibrils also appear thinner due to different tip−sample interactions, especially between the tip and the mica surface. This effect is also shown with the recently introduced surface property mapping technique PeakForce QNM, where the mica surface has very different DMT moduli at different ion concentrations.

Measuring morphological properties of amyloid fibrils with AFM should be done in liquid to avoid dehydration of the sample, depending on the humidity of the environment. Furthermore, the protein conformation might be more readily controlled under liquid conditions. However, even in liquid, comparison of results between protein fibrils is still influenced by environmental scanning conditions. Here we have shown that with careful consideration of different parameters, including solution conditions and AFM

settings, these different results due to influences of scanning conditions can be used to determine structural and conformational information of biological samples at the nanoscale.

MATERIAL AND METHODS

Expression and Purification of α-Synuclein. We performed recombinant expression of wild-type αSYN, the E46K disease mutant, and truncated αSYN(1−108) variants as described before.[7,35] The purification procedure of wild-type and E46K αSYN is the same as previously reported.[7] However, for the 1−108 variant modifications in the standard purification protocol were essential. First, the ammonium sulfate precipitate was dissolved in glycine pH 3.3, and the resulting protein solution was purified using a Resource S column (GE Healthcare Life Sciences, Little Chalfont, United Kingdom). Thereafter, the glycine buffer was exchanged with a desalting step for a 10 mM Tris-HCl pH 7.4 buffer.

Aggregation Reaction. For the height measurements in liquid and air 100 μM solutions of monomeric wild-type, E46K, and αSYN(1−108) in 10 mM Tris-HCl and 50 mM NaCl, pH 7.4, were incubated at 37 °C in glass vials (duplicates) under constant shaking. The aggregation kinetics were monitored using a ThioT fluorescence assay. Samples for AFM measurements were taken when the ThioT fluorescence had just reached its maximum intensity.[5,7]

For the height measurements at varying ion concentrations a second aggregation was performed for wild-type αSYN in the same manner as described above.

Atomic Force Microscopy. *AFM Sample Preparation.* AFM sample preparation was performed by placing 10 μL of a 5 times diluted protein solution on freshly cleaved mica and allowing it to adsorb for 2 min. The sample was washed gently with 200 μL of Milli-Q water and dried carefully under a gentle stream of nitrogen gas for imaging in air. For liquid imaging the sample was not allowed to dry, but was rinsed with the buffer solution. Around 100 μL of fresh buffer was placed on the sample prior to imaging.

Air versus Liquid Measurements. AFM images were made on a Bioscope II (Bruker, Santa Barbara CA, USA) equipped with a silicon probe (cantilever B, k = 1.75 N/m, NSC36, MikroMasch, Tallin, Estonia) for topography imaging in both liquid and ambient air of the full-length and truncated variants. Imaging was performed in tapping mode in ambient air with low force settings (amplitude set point at 35 nm, 80−90% of the free amplitude) to minimize interaction with the sample. For all three α-synuclein variants measured in air one single cantilever was used. In liquid, the amplitude set point was 5 nm, which is 90−95% of the free amplitude. Resonant frequencies were 186 kHz in ambient air and 82 kHz in liquid; see Figure 7A. In liquid, we used a fresh cantilever for every data set for every α-synuclein variant.

Height Measurements at Varying Ion Concentrations. For imaging the wild-type fibrils at varying ion concentrations a custom-built AFM system was used.[50] A silicon nitride MSCT probe, cantilever F (k = 0.5 N/m, Bruker, Santa Barbara, CA, USA), was used with a free amplitude between 1 and 2 nm (amplitude set point between 0.8 and 1.5 nm, 80−90% of the free amplitude). The sample is prepared as described above; however after adsorption the buffer was exchanged with a Tris-HCl buffer only. The ion concentration was then changed after imaging at least 60 fibrils that could be analyzed further. The buffer solution in which the sample is immersed was exchanged with a higher NaCl concentration and left to equilibrate for 30 min. At the higher ion concentrations the resonance frequency and the amplitude set point had to be adjusted due to the increase in density and viscosity to keep similar tapping amplitudes; see Figure 7B. Two different experiments were performed within two different ion concentration ranges. The two different experiments were performed with a fresh cantilever; however during the measurements at different concentrations the cantilever was not changed.

PeakForce QNM Measurements. PeakForce measurements were done on a Bruker Bioscope Catalyst microscope with a Nanoscope V controller (Veeco, Santa Barbara, CA, USA). The analysis software uses the DMT model.[30] The measurements were done in 0.1 M NaCl aqueous solution, in 3 M NaCl aqueous solution, and afterward in ultrapure water. Buffer exchange was similar to the protocol described above in the varying ion concentration section. Previous PeakForce QNM studies on α-synuclein fibrils used a cantilever with a nominal spring constant of 2.8 N/m to determine the modulus of elasticity and maximum force set point of around 2 nN.[21] However, in this study we wanted to measure the subtle differences in tip−sample interaction forces at different ion concentrations. Therefore, we used a less stiff cantilever, MSCT tip F, with a nominal spring constant of 0.5 N/m and a force set point of only 500 pN to be sensitive to the tip−sample interaction forces rather than to the mechanical properties.

Image Morphology Analysis. The average heights of the protein fibrils, measured on top of the fibril along its length, were analyzed using SPIP software (Image Metrology A/S, Lyngby, Denmark) according to the procedure described in ref 7. Only fibrils longer than 100 nm were included in the analysis.

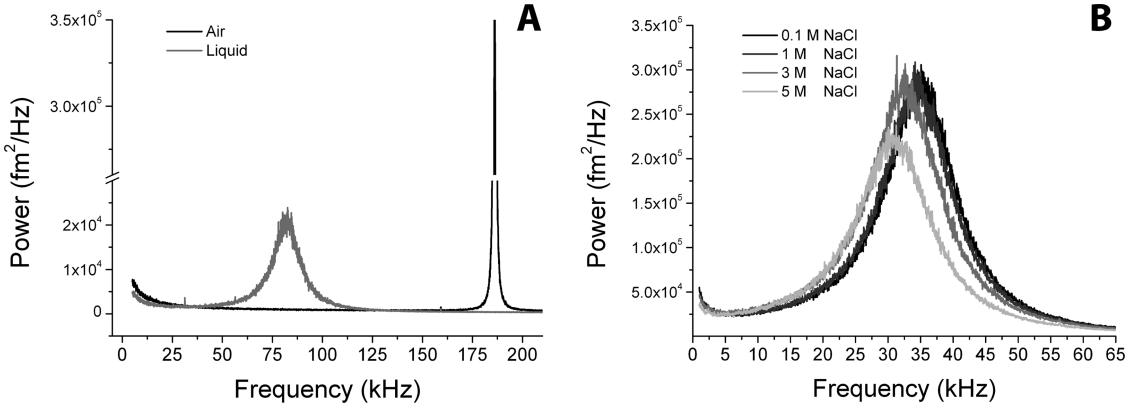

Figure 7. Frequency spectra of (A) NSC36 tip B in air and liquid, resonance frequency dropped from 186.1 kHz in air to 82.0 in liquid, and (B) MSCT tip F in liquid in different ion concentrations. Black curve is in 10 mM Tris and 100 mM NaCl with a frequency of 34.9 kHz. Dark gray curve is at 1 M NaCl, which gave a resonance of 34.2 kHz. NaCl of 3 and 5 M both gave 2 kHz drops in frequency (32.4 and 30.7 kHz). The frequency is lowered due to the increased added mass (density increase), and the cantilever is also more damped (viscosity), resulting in a lower Q.

Conflict of Interest: The authors declare no competing financial interest.

Acknowledgment. The authors thank Kirsten van Leijenhorst-Groener and Marloes ten Haaff-Kolkman for protein expression and purification.

REFERENCES AND NOTES

1. Gosal, W. S.; Myers, S. L.; Radford, S. E.; Thomson, N. H. Amyloid under the Atomic Force Microscope. *Protein Pept. Lett.* **2006**, *13*, 261–270.
2. Knowles, T. P. J.; Buehler, M. J. Nanomechanics of Functional and Pathological Amyloid Materials. *Nat. Nanotechnol.* **2011**, *6*, 469–479.
3. Dobson, C. M. Protein Folding and Misfolding. *Nature* **2003**, *426*, 884–890.
4. Shults, C. W. Lewy Bodies. *Proc. Natl. Acad. Sci. U. S. A.* **2006**, *103*, 1661–1668.
5. Segers-Nolten, I.; van der Werf, K.; van Raaij, M.; Subramaniam, V. Quantitative Characterization of Protein Nanostructures Using Atomic Force Microscopy. *Conf. Proc. IEEE Eng. Med. Biol. Soc.* **2007**, 6609–6612.
6. Khurana, R.; Ionescu-Zanetti, C.; Pope, M.; Li, J.; Nielson, L.; Ramirez-Alvarado, M.; Regan, L.; Fink, A. L.; Carter, S. A. A General Model for Amyloid Fibril Assembly Based on Morphological Studies Using Atomic Force Microscopy. *Biophys. J.* **2003**, *85*, 1135–1144.
7. van Raaij, M. E.; Segers-Nolten, I. M. J.; Subramaniam, V. Quantitative Morphological Analysis Reveals Ultrastructural Diversity of Amyloid Fibrils from α-Synuclein Mutants. *Biophys. J.* **2006**, *91*, L96–L98.
8. Apetri, M. M.; Maiti, N. C.; Zagorski, M. G.; Carey, P. R.; Anderson, V. E. Secondary Structure of α-Synuclein Oligomers: Characterization by Raman and Atomic Force Microscopy. *J. Mol. Biol.* **2006**, *355*, 63–71.
9. Barkhordarian, H.; Emadi, S.; Schulz, P.; Sierks, M. R. Isolating Recombinant Antibodies against Specific Protein Morphologies Using Atomic Force Microscopy and Phage Display Technologies. *Protein Eng. Des. Sel.* **2006**, *19*, 497–502.
10. Bhak, G.; Lee, S.; Park, J. W.; Cho, S.; Paik, S. R. Amyloid Hydrogel Derived from Curly Protein Fibrils of α-Synuclein. *Biomaterials* **2010**, *31*, 5986–5995.
11. Conway, K. A.; Harper, J. D.; Lansbury, P. T., Jr. Fibrils Formed *in Vitro* from α-Synuclein and Two Mutant Forms Linked to Parkinson's Disease Are Typical Amyloid. *Biochemistry* **2000**, *39*, 2552–2563.
12. Crowther, R. A.; Jakes, R.; Spillantini, M. G.; Goedert, M. Synthetic Filaments Assembled from C-Terminally Truncated α-Synuclein. *FEBS Lett.* **1998**, *436*, 309–312.
13. De Franceschi, G.; Frare, E.; Pivato, M.; Relini, A.; Penco, A.; Greggio, E.; Bubacco, L.; Fontana, A.; De Laureto, P. P. Structural and Morphological Characterization of Aggregated Species of α-Synuclein Induced by Docosahexaenoic Acid. *J. Biol. Chem.* **2011**, *286*, 22262–22274.
14. Gai, W. P.; Pountney, D. L.; Power, J. H.; Li, Q. X.; Culvenor, J. G.; McLean, C. A.; Jensen, P. H.; Blumbergs, P. C. α-Synuclein Fibrils Constitute the Central Core of Oligodendroglial Inclusion Filaments in Multiple System Atrophy. *Exp. Neurol.* **2003**, *181*, 68–78.
15. Kim, H. J.; Chatani, E.; Goto, Y.; Paik, S. R. Seed-Dependent Accelerated Fibrillation of α-Synuclein Induced by Periodic Ultrasonication Treatment. *J. Microbiol. Biotechnol.* **2007**, *17*, 2027–2032.
16. Murray, I. V. J.; Giasson, B. I.; Quinn, S. M.; Koppaka, V.; Axelsen, P. H.; Ischiropoulos, H.; Trojanowski, J. Q.; Lee, V. M.-Y. Role of α-Synuclein Carboxy-Terminus on Fibril Formation in Vitro. *Biochemistry* **2003**, *42*, 8530–8540.
17. Qin, Z.; Hu, D.; Han, S.; Hong, D. P.; Fink, A. L. Role of Different Regions of α-Synuclein in the Assembly of Fibrils. *Biochemistry* **2007**, *46*, 13322–13330.
18. Volkova, K. D.; Kovalska, V. B.; Yu Losytskyy, M. Y.; Veldhuis, G.; Segers-Nolten, G. M. J.; Tolmachev, O. I.; Subramaniam, V.; Yarmoluk, S. M. Studies of Interaction Between Cyanine Dye T-284 and Fibrillar Alpha-Synuclein. *J. Fluoresc.* **2010**, *20*, 1267–1274.
19. Zhang, F.; Lin, X.; Ji, L. N.; Du, H. N.; Tang, L.; He, J. H.; Hu, J.; Hu, H. Y. Assembly of α-Synuclein Fibrils in Nanoscale Studied by Peptide Truncation and AFM. *Biochem. Biophys. Res. Commun.* **2008**, *368*, 388–394.
20. Hoyer, W.; Antony, T.; Cherny, D.; Heim, G.; Jovin, T. M.; Subramaniam, V. Dependence of α-Synuclein Aggregate Morphology on Solution Conditions. *J. Mol. Biol.* **2002**, *322*, 383–393.
21. Sweers, K. K. M.; van der Werf, K. O.; Bennink, M. L.; Subramaniam, V. Nanomechanical Properties of α-Synuclein Amyloid Fibrils: A Comparative Study by Nanoindentation, Harmonic Force Microscopy, and PeakForce QNM. *Nanoscale Res. Lett.* **2011**, *6*, 270.
22. Keller, A.; Fritzsche, M.; Yu, Y. P.; Liu, Q.; Li, Y. H.; Dong, M.; Besenbacher, F. Influence of Hydrophobicity on the Surface-Catalyzed Assembly of the Islet Amyloid Polypeptide. *ACS Nano* **2011**, *5*, 2770–2778.
23. Moreno-Herrero, F.; Pérez, M.; Baró, A. M.; Avila, J. Characterization by Atomic Force Microscopy of Alzheimer Paired Helical Filaments under Physiological Conditions. *Biophys. J.* **2004**, *86*, 517–525.
24. Chamberlain, A. K.; Macphee, C. E.; Zurdo, J.; Morozova-Roche, L. A.; Hill, H. A.; Dobson, C. M.; Davis, J. J. Ultrastructural Organization of Amyloid Fibrils by Atomic Force Microscopy. *Biophys. J.* **2000**, *79*, 3282–3293.
25. Nikiforov, M. P.; Thompson, G. L.; Reukov, V. V.; Jesse, S.; Guo, S.; Rodriguez, B. J.; Seal, K.; Vertegel, A. A.; Kalinin, S. V. Double-Layer Mediated Electromechnical Response of Amyloid Fibrils in Liquid Environment. *ACS Nano* **2010**, *4*, 689–698.
26. Song, Y.; Bhushan, B. Finite-Element Vibration Analysis of Tapping-Mode Atomic Force Microscopy in Liquid. *Ultramicroscopy* **2007**, *107*, 1095–1104.
27. Goedert, M. Alpha-Synuclein and Neurodegenerative Diseases. *Nat. Rev. Neurosci.* **2001**, *2*, 492–501.
28. Zarranz, J. J.; Alegre, J.; Gómez-Esteban, J. C.; Lezcano, E.; Ros, R.; Ampuero, I.; Vidal, L.; Hoenicka, J.; Rodriguez, O.; Atarés, B.; *et al*. The New Mutation, E46K, of α-Synuclein Causes Parkinson and Lewy Body Dementia. *Ann. Neurol.* **2004**, *55*, 164–173.
29. Pittenger, B.; Erina, N.; Su, C. Quantitative Mechanical Property Mapping at the Nanoscale with PeakForce QNM. Application Note, Veeco Instruments Inc., 2010
30. Derjaguin, B. V.; Muller, V. M.; Toporov, Yu. P. Effect of Contact Deformations on Adhesion of Particles. *J. Colloid Interface Sci.* **1975**, *53*, 314–326.
31. Young, T. J.; Monclus, M. A.; Burnett, T. L.; Broughton, W. R.; Ogin, S. L.; Smith, P. A. The Use of the PeakForce Quantitative Nanomechanical Mapping AFM-Based Method for High-Resolution Young's Modulus Measurement of Polymers. *Meas. Sci. Technol.* **2011**, *22*, 125703.
32. Tan, J. C.; Saines, P. J.; Bithell, E. G.; Cheetham, A. K. Hybrid Nanosheets of an Inorganic-Organic Framework Material: Facile Synthesis, Structure and Elastic Properties. *ACS Nano* **2012**, *6*, 615–621.
33. Adamcik, J.; Berquand, A.; Mezzenga, R. Single-Step Direct Measurement of Amyloid Fibrils Stiffness by Peak Force Quantitative Nanomechanical Atomic Force Microscopy. *Appl. Phys. Lett.* **2011**, *98*, 193701.
34. Ban, T.; Hamada, D.; Hasegawa, K.; Naiki, H.; Goto, Y. Direct Observation of Amyloid Fibril Growth Monitored by Thioflavin T Fluorescence. *J. Biol. Chem.* **2003**, *278*, 16462–16465.
35. Hoyer, W.; Cherny, D.; Subramaniam, V.; Jovin, T. M. Impact of the Acidic C-Terminal Region Comprising Amino Acids 109−140 on α-Synuclein Aggregation *in Vitro*. *Biochemistry* **2004**, *43*, 16233–16242.
36. Goldsbury, C.; Goldie, K.; Pellaud, J.; Seelig, J.; Frey, P.; Müller, S. A.; Kistler, J.; Cooper, G. J. S.; Aebi, U. Amyloid Fibril Formation from Full-Length and Fragments of Amylin. *J. Struct. Biol.* **2000**, *130*, 352–362.
37. van Noort, S. J. T.; van der Werf, K. O.; de Grooth, B. G.; van Hulst, N. F.; Greve, J. Height Anomalies in Tapping Mode Atomic Force Microscopy in Air Caused by Adhesion. *Ultramicroscopy* **1997**, *69*, 117–127.

38. Santos, S.; Barcons, V.; Christenson, H. K.; Font, J.; Thomson, N. H. The Intrinsic Resolution Limit in the Atomic Force Microscope: Implications for Heights of Nano-Scale Features. *PloS One* **2011**, *6*, e23821.
39. Weisenhorn, A. L.; Hansma, P. K.; Albrecht, T. R.; Quate, C. F. Forces in Atomic Force Microscopy in Air and Water. *Appl. Phys. Lett.* **1989**, *54*, 2651–2653.
40. Farshchi-Tabrizi, M.; Kappl, M.; Butt, H. J. Influence of Humidity on Adhesion: An Atomic Force Microscopy Study. *J. Adhes. Sci. Technol.* **2008**, *22*, 181–203.
41. Goodman, F. O.; Garcia, N. Roles of Attractive and Repulsive Forces in Atomic-Force Microscopy. *Phys. Rev. B* **1991**, *43*, 4728–4731.
42. Butt, H. J.; Capella, B.; Kappl, M. Force Measurements with the Atomic Force Microscope: Technique, Interpretation and Applications. *Surf. Sci. Rep.* **2005**, *59*, 1–152.
43. Vilar, M.; Chou, H.; Lührs, T.; Maji, S. K.; Riek-Loher, D.; Verel, R.; Manning, G.; Stahlberg, H.; Riek, R. The Fold of α-Synuclein Fibrils. *Proc. Natl. Acad. Sci. U. S. A.* **2008**, *105*, 8637–8642.
44. Sunde, M.; Serpell, L. C.; Bartlam, M.; Fraser, P. E.; Pepys, M. B.; Blake, C. C. F. Common Core Structure of Amyloid Fibrils by Synchrotron X-Ray Diffraction. *J. Mol. Biol.* **1997**, *273*, 729–739.
45. Ghosh, K.; Dill, K. A. Computing Protein Stabilities from their Chain Lengths. *Proc. Natl. Acad. Sci. U. S. A.* **2009**, *106*, 10649–10654.
46. Fitzkee, N. C.; Rose, G. D. Reassessing Random Coil Statistics in Unfolded Proteins. *Proc. Natl. Acad. Sci. U. S. A.* **2004**, *101*, 12497–12502.
47. Hoh, J. H.; Revel, J.; Hansma, P. K. Tip-Sample Interactions in Atomic Force Microscopy: I. Modulating Adhesion between Silicon Nitride and Glass. *Nanotechnology* **1991**, *2*, 119–122.
48. Senden, T. J.; Drummond, C. J. Surface Chemistry and Tip-Sample Interactions in Atomic Force Microscopy. *Colloid Surf. A* **1995**, *94*, 29–51.
49. Ebeling, D.; van den Ende, D.; Mugele, F. Electrostatic Interaction Forces in Aqueous Salt Solutions of Variable Concentration and Valency. *Nanotechnology* **2011**, *22*, 305706.
50. van der Werf, K. O.; Putman, C. A. J.; de Grooth, B. G.; Segerink, F. B.; Schipper, E. H.; van Hulst, N. F.; Greve, J. Compact Stand-Alone Atomic Force Microscope. *Rev. Sci. Instrum.* **1993**, *64*, 2892–2897.